THE ASTROPHYSICAL JOURNAL, 419:739–745, 1993 December 20

VOYAGER OBSERVATIONS OF DIFFUSE FAR-ULTRAVIOLET CONTINUUM AND LINE EMISSION IN ERIDANUS

JAYANT MURTHY[1], M. IM, AND R. C. HENRY
Department of Physics and Astronomy, The Johns Hopkins University, Baltimore, MD 21218
AND
J. B. HOLBERG
Lunar and Planetary Laboratory, University of Arizona, Tucson, AZ 85721
Received 1992 June 18; accepted 1993 June 28

ABSTRACT

We present *Voyager* observations of the diffuse far-ultraviolet radiation field (912 Å–1150 Å) in two regions of the Eridanus superbubble. A strong continuum is present in both locations which we have identified with starlight scattered by interstellar dust. From the level of this emission (1620 ± 150 photons cm^{-2} s^{-1} sr^{-1} $Å^{-1}$) we have placed a lower limit of about 0.3 on the albedo if the scattering is isotropic and an upper limit of about 0.8 on the phase function asymmetry factor (g) if the grains are perfectly reflecting. In addition, O VI ($\lambda\lambda$ 1032/1038) emission with an intensity of $28.7 \pm 2.8 \times 10^4$ photons cm^{-2} s^{-1} sr^{-1} is apparent in one of the two locations, and C III (977 Å) is visible in both locations with intensities of $2.14 \pm 0.75 \times 10^4$ and $18.9 \pm 1.7 \times 10^4$ photons cm^{-2} s^{-1} sr^{-1}. The line ratios indicate shock velocities on the order of 90 km s^{-1} in one of the targets and 180 km s^{-1} in the other, which is located near a peak of the C-band X-ray emission.
Subject headings: diffuse radiation — ISM: bubbles — ISM: individual (Eridanus) — ultraviolet: interstellar

1. INTRODUCTION

As part of our program to map the diffuse ultraviolet radiation field, we have obtained the first far-ultraviolet spectra of two locations (Table 1) in the Eridanus superbubble. This region which was first discovered as an X-ray "hot spot" of more than 15° in extent (Williamson et al. 1974; Naranan et al. 1976), is delineated by an expanding shell of H I with a radius of 20° (Heiles 1976). Both diffuse and filamentary Hα emission can be seen throughout the region (Sivan 1974; Reynolds, Roessler, & Scherb 1974) and intense emission in the near-UV was noted by Paresce, Jakobsen, & Bowyer (1983). It is now generally accepted that these phenomena along with such structures as Barnard's Loop in Orion, are due to the Eridanus superbubble, blown by one or more supernovae in the Orion OB association and now possibly maintained by the intense stellar winds from those stars (Reynolds & Ogden 1979).

Our observations were made with the ultraviolet spectrometer (UVS) aboard the *Voyager 2* spacecraft, now well beyond the orbit of Neptune and conducting an active program of astronomical observations (see Holberg 1991 for a full description of the spacecraft and instrumentation). The UVS has a resolution of 38 Å (for diffuse sources) between 525 and 1650 Å with a field of view of 0°.10 × 0°.87. The spectral region of greatest interest to us is in the region between 912 Å, the Lyman limit, and about 1150 Å, at which point the intense solar system Lyα line dominates any signal we might expect to see. At longer wavelengths, above Lyα, the sensitivity of the bare microchannel plate is too low to detect most diffuse emissions.

The exact locations of our observations (Table 1) were chosen such that there were no known hot stars in, or near, the field of view. This was initially verified using several catalogs including SKYMAP (Gottlieb 1978), the Smithsonian Astrophysical Observatory (SAO) catalog, the TD-1 survey, and a bibliographic search of the two regions using the SIMBAD database. It is important to note that no stars, no matter how bright, of spectral type A2 or later will yield a detectable signal in the UVS channels below Lyα. Spatial binning of the observed spectra as a function of the limit cycle motion of the spacecraft showed no evidence of the characteristic signature of point sources (Holberg & Watkins 1992). This is a very sensitive test for the presence of point sources which is routinely used to detect and extract stellar spectra of hot stars as faint as 15th magnitude in UVS data. We estimate that no more than 20% of the signal in target A, the fainter of the two locations, could arise from unresolved stellar sources.

A diffuse continuum, due to starlight scattered from interstellar dust in the line of sight, is apparent in both targets. Line emission from O VI (1032/1038 Å) is present in one of the locations observed while emission from C III (977 Å) is present in both targets. Although both these lines have been observed in the Cygnus Loop (Shemansky, Sandel, & Broadfoot 1978; Blair et al. 1991a) and Vela supernova remnants (W. P. Blair, personal communication), this is the first reported detection of these lines from regions of the interstellar medium not clearly associated with the bright filaments of supernova remnants. We have examined soft X-ray maps of the region (kindly provided by D. B. Burrows) and it is apparent that, although both targets are in a region of excess emission, target B, in particular, is locted very near a peak in the C-band emission, which traces gas of the same temperature as that in which the O VI is produced.

2. DATA ANALYSIS

The data analysis follows that of Holberg (1986) and Murthy, Henry, & Holberg (1991). The basis for our procedure is that the integrated UVS spectrum can be decomposed into three parts: an instrumental dark count, due primarily to radiation from the spacecraft's radioisotope thermoelectric gener-

[1] Guest Observer with the *Voyager* Ultraviolet Spectrometers.

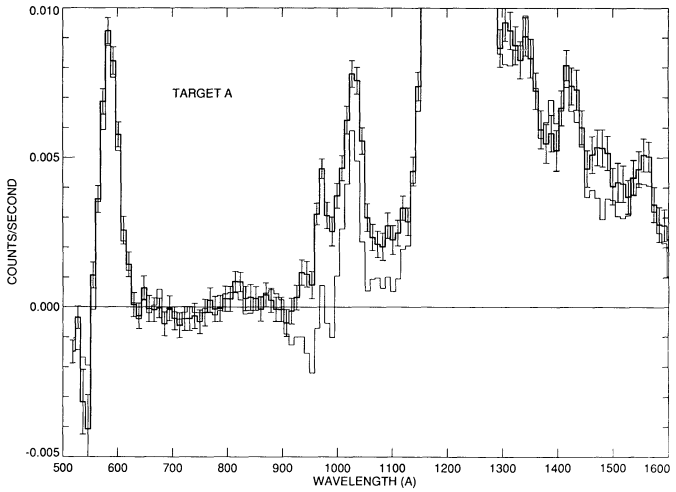

FIG. 1a

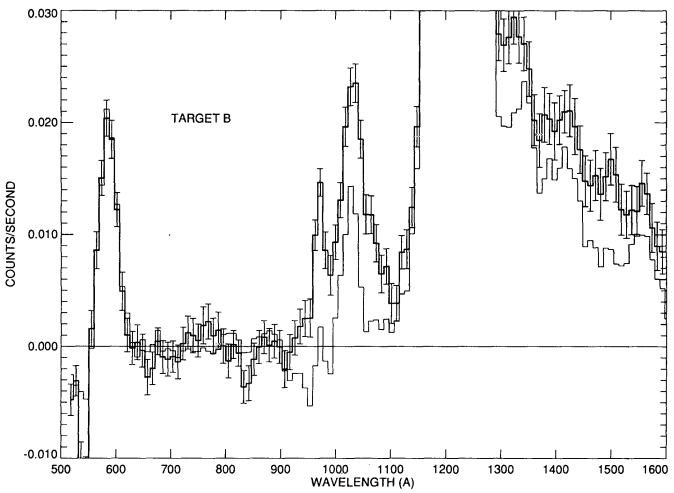

FIG. 1b

FIG. 1.—We have plotted the observed profile toward both Target A and Target B as dark lines with $\pm 1\ \sigma$ error bars. The scaled template profile, which fits the solar system emission lines, is plotted as the thin line. Note the excellent fit to the interplanetary Heα feature at 584 Å. There is clear evidence for a strong cosmic signal in both targets, with both continuum and line emission present. Most of the signal in the template at wavelengths greater than Lyα is due to instrumentally scattered heliospheric Lyα.

TABLE 1

OBSERVATION LOG

Target	l	b	Observation (Date)	Exposure Time (s)	Log [N(H I)][a] (cm^{-2})
A.....	197.3	−49.2	1989 Sep 10	208,512	20.57
B.....	190.0	−45.0	1991 Oct 18	354,183	20.76

[a] Stark et al. 1992.

ator (RTG); emission lines from resonantly scattered solar radiation; and a residual containing any astrophysical signal. The shape of the dark count spectrum has been independently determined from observations of a shadowed region on the spacecraft (Holberg 1986), and the level was unambiguously set from the spectral region below the Lyman limit (912 Å), where the opacity of the ISM is so high that no astrophysical signal will be seen. Following the dark count subtraction, instrumental scattering was removed by applying a matrix operator, determined from preflight calibrations. These spectra, which are dominated by the interplanetary lines of H I Lyα (1216 Å) and Lyβ (1026 Å), and He I (584 Å), are plotted in Figure 1.

In order to model the interplanetary lines, we constructed a template spectrum out of a weighted four observations in which no cosmic signal was detected. Three of these are targets A, B, and D of Murthy et al. (1991) (their target C was rejected because of evidence for a weak cosmic signal); the other was taken as part of an unsuccessful attempt to observe emission from the high-latitude optical nebulosity first detected by Sandage (1976). The template was scaled to our observations

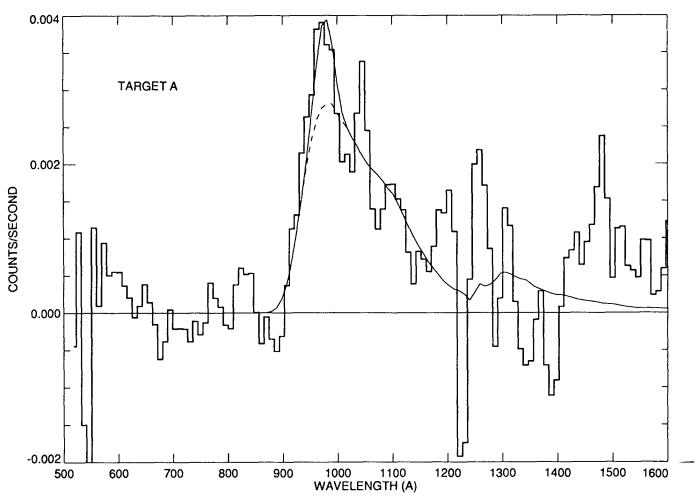

FIG. 2a

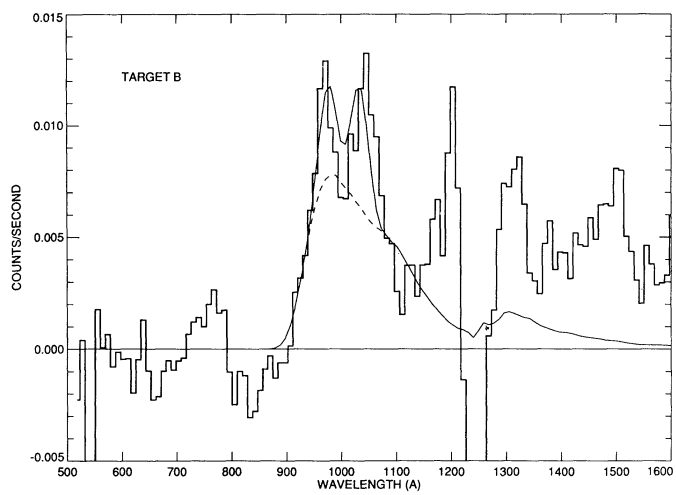

FIG. 2b

FIG. 2.—The residuals after subtraction of the template are plotted as dark lines for both targets. Note the different vertical scales for each plot. The thin line through the plots represents our best-fit model, including a scattered light continuum (*dashed line*), a C III line at 977 Å, and an O VI doublet at 1032/1038 Å. The continuum level is almost thrice as high in Target B as in Target A; which is unlikely to be correct for locations only 10° apart with approximately the same physical conditions.

using a least-squares method and subtracted. We have checked the consistency of our template spectrum by applying it to each of its components and have found no residuals. This technique has been successfully used in the analysis of many *Voyager* observations, including more than two dozen observations of the diffuse radiation field (Holberg 1990; Murthy et al. 1991).

We have plotted the residuals after subtraction of the template in Figure 2. In practice, rather than subtracting the template and fitting the residuals, we fit all of the different components simultaneously. There is a strong continuum in both targets, which cuts off at 912 Å (or, actually, slightly below 912 Å because of the instrumental resolution) as any well-behaved cosmic signal should do, and, in addition, at least two lines in the spectrum of target B and one line in target A. The low resolution of the UVS renders it difficult to fully decompose the observed signal into its components and we will discuss our modeling techniques below. There is also emission at wavelengths above Lyα in target B; however, because of the relatively low sensitivity of the UVS in that region the uncertainties are large and we will concentrate our efforts in the band below 1200 Å. (The nonzero emission in the template spectrum at wavelengths greater than Lyα is largely due to internal scattering of Lyα photons in the instrument.)

3. MODELING

The most obvious source of diffuse continuum emission in this wavelength regime is starlight scattered by interstellar dust. We have developed a general model to predict the amount of this radiation as a function of look direction (see Murthy et al. 1991 for a full discussion). This model divides the line of sight into a number of equal cells and calculates the radiation field at each cell using all the O, B, and A stars in SKYMAP (Gottlieb 1978). The total amount of dust in the line of sight is distributed among the individual cells, and the incident starlight is then scattered off each cell. The scattered light seen at the Earth is simply the sum of the contributions from each cell attenuated by the dust between that cell and the observer.

We have used the Bell Labs H I survey (Stark et al. 1992) with the canonical gas-to-dust ratio of $N(H)/E(B-V) = 5.8 \times 10^{21}$ cm^{-2} mag^{-1} (Bohlin, Savage, & Drake 1978) to estimate the total amount of dust in the direction of each of our target (see Table 1). There are a few stars in the general vicinity of our target positions with the measured H I column densities or with a known extinction and these are listed in Table 2. The closest of these stars to us (γ Ori), at a distance of 110 pc, has a column density of between $10^{18.3}$ and $10^{19.3}$ cm^{-2} while the other stars have essentially identical column densities of about $10^{20.5}$ cm^{-2}, although their distances range from 230 pc to 465 pc. Hence we have assumed that all of this gas, which forms the near edge of the Eridanus superbubble, is located at a distance of 200 pc. The far edge of the bubble is located at a distance of about 500 pc with a column density of about 10^{20} cm^{-2} (Burrows et al. 1993).

TABLE 2

STARS NEAR THE TWO TARGETS

Star	l	b	d (pc)	log [N(H I)]
γ Ori	197	−16	110	18.3–19.3
π Ori	196	−25	230	20.41
HD 29248	198	−31	275	20.52
HD 16582	171	−52	248	20.36
HD 28497	208	−37	465	20.30
HD 25400	190	−39	185	20.97

NOTE.—All data from Shull & van Steenberg 1984, except for γ Ori (Paresce 1984) and HD 25400 (Penprase et al. 1990).

The incident starlight is dependent on the extinction assumed in the intervening interstellar medium. Burrows et al. (1993) have recently published a schematic of the Eridanus superbubble in which there is essentially no attenuation between the H II shell (which they place at a distance of about 150 pc) and the Orion OB association. We have implemented this by assuming no attenuation of the radiation from stars in Orion ($185 < l < 210$; $-50 < b < -10$) while assuming a standard extinction corresponding to $A_V = 1$ mag kpc^{-1} ($n_H = 0.6$ cm^{-3}) for all other stars. The scattered radiation predicted by our model in the direction of Target A is plotted for different values of g in Figure 3 assuming an albedo of 0.1. As only single scattering is present in our model, the level of the scattered light is directly proportional to the albedo.

It is clear from Figures 1 and 2 that there are two lines present in the spectrum of Target B, but the exact strength and position of these lines is dependent on the level and shape of the assumed continuum. Our spectra are superficially similar to the *Voyager* spectra of the Cygnus Loop (Shemansky et al. 1978; Blair et al. 1991b). Using higher resolution (~5 Å) data from the Hopkins Ultraviolet Telescope (HUT), Blair et al. (1991a) have conclusively identified as consisting primarily of C III (λ 977 Å) and O VI ($\lambda\lambda$ 1032/1038 Å) with some contribution from N III (λ 991 Å). The features in our spectrum are actually fitted rather poorly by lines at these positions, with centroids differing by about 10 Å (one spectral channel) from the laboratory values. Similar shifts have been seen in the much brighter spectra in the Cygnus Loop but, as has been discussed by those authors, there are no other viable contenders for those identifications. We will discuss this further in the next section.

Our model spectrum consists of the dust-scattered radiation predicted by our simulation described above plus emission lines at the nominal positions of C III (977 Å) and O VI (1032/1038 Å), with the peak strength of the 1032 Å line fixed to be twice that of the 1038 Å line. A least-squares procedure was

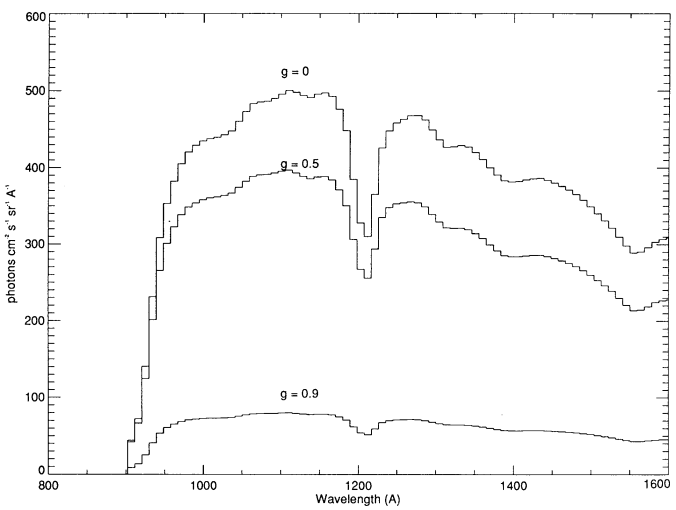

FIG. 3.—The spectral dependence of our predicted dust scattering is plotted for three values of g assuming an albedo of 0.1. As our model includes only single-scattering, the level of the emission will scale directly as the albedo.

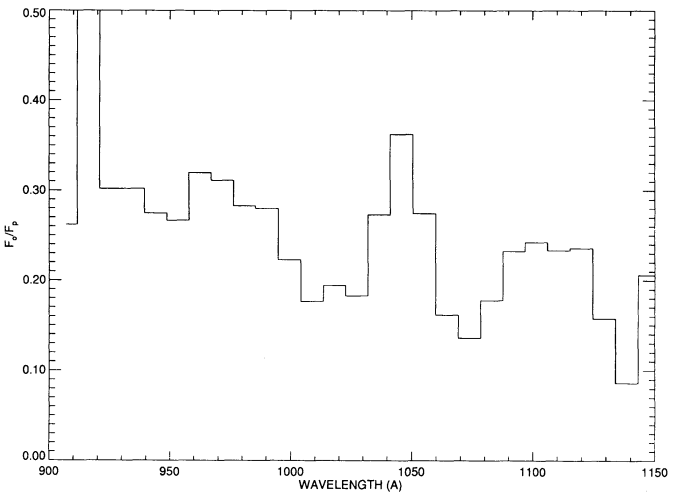

FIG. 4.—The ratio of the observed flux to that predicted by our dust-scattering model (with an albedo of unity and $g = 0$) is shown. This plot is therefore an upper limit on the albedo for isotropic scatterers. There is some tendency for an increase in the ratio to shorter wavelengths; however, we believe it is more likely that the apparent increase in the albedo is caused by the presence of the C III emission line (the 38 Å FWHM of the spectrometer spreads out the line from 940 Å to 1020 Å). Note that because the sensitivity drops so rapidly with increasing wavelength, random noise at long wavelengths will appear as emission lines of the same intensity as those lines below Lyα.

then used to fit the data with the normalization of the continuum and the two emission lines as free parameters. There is an implicit assumption in this procedure that the optical constants of the dust do not change much over the approximately 200 Å range in which the continuum is a significant part of our observed signal, even though the extinction curve continues to rise sharply (Snow, Allen, & Polidan 1990). A crude measure of the effective albedo as a function of wavelength is simply the ratio of the observed signal to that predicted by our model and we have plotted this ratio for Target A, assuming isotropic scattering, in Figure 4. There is some evidence for an increase in the ratio toward shorter wavelengths, part of which is due to the putative feature at 980 Å. In order to allow for this possibility, we considered our model in which the albedo was allowed to rise linearly from 1200 Å to 912 Å. Our results are summarized in Table 3 and will be discussed in the next section.

4. RESULTS

If we assume that there are no lines present, the best-fit value for the continuum in Target A is 1950 ± 80 photons cm^{-2} s^{-1} sr^{-1} $Å^{-1}$ at 1100 Å. (Note that, as the shape of the continuum is fixed, we only need to specify its value at one wavelength.) A significantly better fit can be achieved by adding the C III line at 977 Å with an intensity of 2.14 ± 0.66 × 10^4 photons cm^{-2} s^{-1} sr^{-1}, and this model is shown as the thin solid line in Figure 2*a*. However, we obtained an equally good fit by allowing the albedo (at a constant g) to increase linearly by a factor of 1.6 between 1100 Å and 900 Å, with no lines. Recent observations of dust scattering in the reflection nebula NGC 7023 (Murthy et al. 1993; Witt et al. 1993) have shown that the ratio between the incident and scattered radiation is constant over the entire spectral range and we therefore believe that the first alternative, the presence of a C III emission line, is more likely to be correct, especially as we unequivocally detect both C III and O VI in Target B.

We have plotted the prediction of our model for the scattered light in Target A as a function of the optical constants a and g in Figure 5. The data force the optical constants to be bounded approximately by the 1400 and 1800 photon cm^{-2} s^{-1} sr^{-1} $Å^{-1}$ contours, placing a lower limit of about 0.3 on the albedo and an upper limit of 0.8 on g. If, in addition, we force the albedo to be below 0.5, we can restrict g to lie below about 0.6. While we believe that our model is reasonably accurate, we note that errors in our assumptions in either the dust distribution or the radiation field will affect our predictions for the scattered light and hence our derivation of the optical constants.

There are very few observational constraints on the optical properties of the dust below Lyα. Murthy et al. (1991) have placed an upper limit of 0.1 on the albedo of the grains, unless g is very high (>0.95), based on *Voyager* observations of four lines of sight (three of which have been incorporated into our template) in which no diffuse radiation was detected. Our model for the scattered light was in its early stages at the time with incomplete stellar and dust distributions. We plan to reanalyze these old spectra with our current, more evolved, model

TABLE 3

RESULTS

Model	Reduced χ^2 (degrees of freedom)	Continuum Intensity[a]	C III (977 Å) Intensity[b]	O VI (1032/1038 Å) Intensity[b]
		Target A		
M-1	1.03 (46)	1950 ± 80		
M-2	0.81 (45)	1700 ± 110	2.14 ± 0.75	
M-3	0.81 (44)	1620 ± 150	2.47 ± 0.75	0.96 ± 1.07
M-4	0.81 (45)	1500		
		Target B		
M-1	2.27 (46)	6500 ± 300		
M-3	1.98 (44)	4900 ± 400	7.56 ± 2.52	14.2 ± 3.6
M-5	2.77 (45)	1720	18.9 ± 1.7	28.7 ± 2.8

NOTE.—Model M-1 includes only a dust scattered continuum; model M-2 includes a continuum plus the C III line; model M-3 is the same as model M-2 but with an additional O VI line; model M-4 allows for a sloped albedo with no lines; and model M-5 assumes the continuum normalization found in Target A.

[a] Photons cm^{-2} s^{-1} sr^{-1} $Å^{-1}$ at 1100 Å.

[b] 10^4 photons cm^{-2} s^{-1} sr^{-1}.

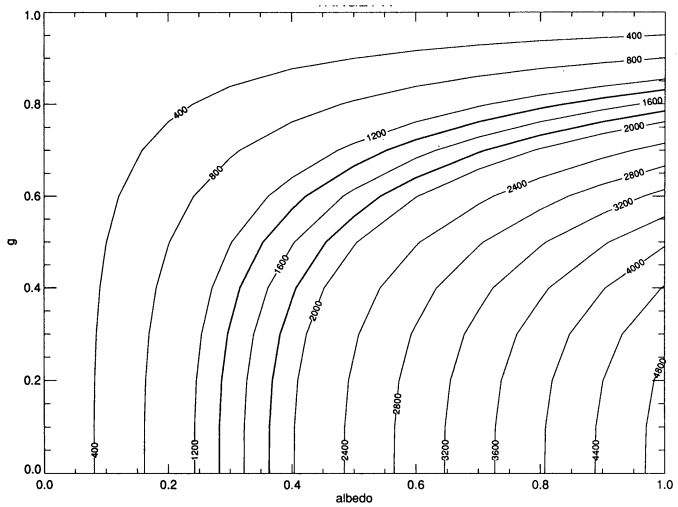

FIG. 5.—We have plotted the amount of dust scattered light predicted by our model in Target A as a function of a and g. Our observed value for the continuum is 1600 ± 150 photons cm^{-2} s^{-1} sr^{-1} Å^{-1} from which we can roughly constrain the two parameters to lie between the 1400 and 1800 photons cm^{-2} s^{-1} sr^{-1} Å^{-1} contours (the two dark lines).

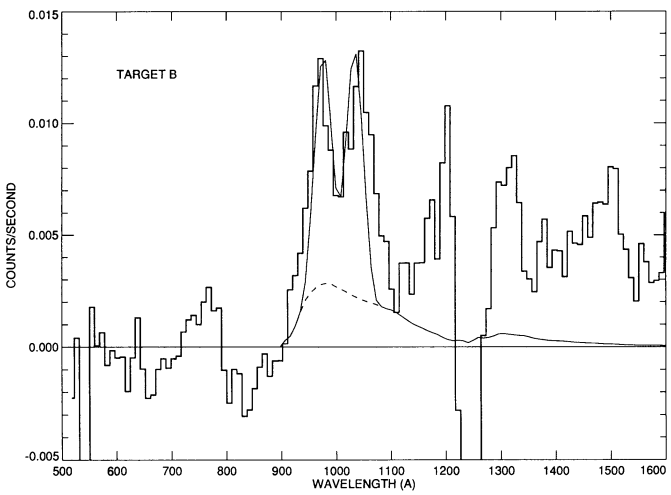

FIG. 6.—This plot is analogous to Fig. 3 except that the continuum has been fixed using the normalization between the predicted and observed background level in Target A. The χ^2 of this fit is much worse than the best-fit case, largely because the emission lines are poorly fitted. However, we believe that this simulation is more realistic because we do not expect the dust-scattered continuum to vary by a factor of 3 between the two locations. Note the good fit to the valley between the two lines.

to determine whether the variations could be due to uncertainties in the model or are real. The only other limits in this spectral regime have come from observations of NGC 7023 using the HUT (Murthy et al. 1993) and *Voyager 2* (Witt et al. 1993). Witt et al. have derived an albedo of 0.41 with $g = 0.75$ at 1100 Å. However, this result is rather model-dependent and Murthy et al. have shown that, with different assumptions, the data are consistent with an albedo as low as 0.2. It should also be noted that there are considerable variations in the extinction curve in different regions of the sky (Fitzpatrick & Massa 1988) and thus, a priori, one may expect that the optical constants of the grains vary in a like manner.

A much higher continuum of 4900 ± 500 photons cm^{-2} s^{-1} sr^{-1} Å^{-1} was found in Target B. This is almost thrice the level in Target A, which is about 10° away. Our model, which takes into account the different radiation fields in the two locations, predicts that the scattered light should be only about 15% higher with the same optical constants. If all of this higher continuum is due to dust-scattered starlight, then either the optical constants must be much different between the two regions or the dust must be highly clumped in Target A; i.e., it fills a much smaller fraction of the *Voyager* slit. Given our assumption that the scattering in both locations arises in the H I shell around the bubble, it seems unlikely that the physical conditions in the two targets are grossly different and we therefore believe that the higher apparent continuum is an artifact of the poor spectral resolution of the instrument.

We have fixed the level of the continuum in Target B using our model and normalizing by the same factor as found in Target A and allowed only the strengths of the lines to vary. The resulting strengths of the emission lines are listed in Table 4 and the fit plotted in Figure 6. Although the χ^2 is much worse than the best-fit case, we believe that this representation of the data, in which we assume that there is little difference between the physical properties of the dust in the two locations, is the more realistic. A comparison between Figures 6 and 2*b* illustrates the reason for the high χ^2. The two line features are apparently shifted somewhat in wavelength and are broader than the nominal 38 Å FWHM of the instrument, and the least-squares procedure compensates by increasing the continuum to fit the sides of the lines. Note that the valley between the two features is fitted rather poorly by the best-fit model.

If we allow the strength and FWHM of the two lines in Target B to vary (while still normalizing the continuum to Target A) we find that the best-fit position of the C III feature is at 968 Å with a FWHM of 47 Å, and the O VI doublet is centered at 1047 Å with a FWHM of 60 Å, now with a χ^2 close to the best-fit case. If the same procedure is used with Target A, the C III feature is shifted to 965 Å with a FWHM of 47 Å, although the improvement in χ^2 is not as dramatic. Similar effects were noted in the *Voyager* observations of the Cygnus Loop (Shemansky et al. 1979; Blair et al. 1991b) and line blending was suggested as a possible explanation. However, there is no evidence for other lines in the HUT spectra (Blair et al. 1991a). A possibility is that nonuniform emission in the slit might cause the line shape to deviate sufficiently from the nominal 38 Å Gaussian that a Gaussian profile is no longer appropriate, leading to incongruous results.

As discussed above, we have estimated the $E(B-V)$ to the emitting regions in both Target A and Target B to be about 0.05. This leads to a total flux at the source of $9.9 \pm 3.1 \times 10^{-7}$ ergs cm^{-2} s^{-1} sr^{-1} in the C III line in Target A and fluxes of $11.5 \pm 0.8 \times 10^{-6}$ ergs cm^{-2} s^{-1} sr^{-1} and $14.2 \pm 1.1 \times 10^{-6}$ ergs cm^{-2} s^{-1} sr^{-1} for the C III and O VI lines (with the contin-

TABLE 4

LINES PREDICTED ABOVE 1200 Å FOR TARGET B

Emission Line	Flux[a]
N V (1240 Å)	4.0×10^5
C II (1336 Å)	1.7×10^5
Si IV (1397 Å)	5.0×10^4
O IV (1402 Å)	3.6×10^5
C IV (1549 Å)	9.6×10^5

[a] Photons cm^{-2} s^{-1} sr^{-1} from Hartigan et al. 1987 scaled to C III for a shock of 180 km s^{-1}.

uum normalized to that of Target A), respectively, in Target B. The O VI to C III ratio is a sensitive indicator of the shock velocity: below 160 km s^{-1} virtually no O VI is produced while above 180 km s^{-1} the O VI to C III ratio increases to a factor of 6 or more (Hartigan, Raymond, & Hartmann 1987). As the ratio in Target B is close to unity, the shock velocities must be on the order of 160–180 km s^{-1}. At these velocities, and again using the models of Hartigan et al., we deduce an Hα emission of 4.5×10^{-6} ergs cm^{-2} s^{-1} sr^{-1}, corresponding to 18 rayleighs (R). This is entirely consistent with the 20 R of Hα detected by Reynolds & Ogden (1979) in the vicinity of both targets, with a velocity of about 20 km s^{-1}. The only significant difference if we use the best-fit model for the continuum is that the Hα emission would be only about 7 R in Target B, much lower than that observed. The shock velocities in Target A must be much lower as there is no evidence for the presence of O VI and, in fact, the C III/Hα ratio of about 0.3 indicates that the velocities must be on the order of 90 km s^{-1}, the turn-on velocity for the production of C III. While the uncertainty in the level of the continuum translates into a large uncertainty in the strengths of the emission lines, the very presence of the lines leaves little ambiguity in the shock velocities derived.

Although emission above Lyα is clearly present in the spectrum of Target B, we have not fitted that region, primarily because the sensitivity of the instrument drops so much above Lyα that random noise effects dominate the spectrum. Our predicted dust-scattered component (plotted in Fig. 6) is much too low to explain this emission; also note that no long-wavelength emission is detected in Target A. In addition to scattered starlight, we also expect emission lines from other species excited by the shocks present (Table 4) and two photon emission from the radiative decay of H I (Tucker & Koren 1971). We have plotted a composite profile containing all these sources in Figure 7. Although still not a good fit above Lyα, the quality of the data, as attested by the size of the error bars, in this spectral region does not warrant a more detailed analysis.

Paresce et al. (1983) claimed a generally high level of emission in Eridanus, including an intensity of 6000 units at the location of Target A, using a photometer with a spectral range of 1350–1750 Å aboard a sounding rocket. At a shock velocity of 90 km s^{-1} only 51 photons cm^{-2} s^{-1} sr^{-1} $Å^{-1}$ (units) are predicted in the 1350–1750 Å range by the models of Hartigan et al. (1987); however, if we increase the shock velocity to 120 km s^{-1} the source emission rises dramatically to about 7300 units, primarily because C IV turns on. Taking the reddening into account, this translates to an intensity of about 4700 units at the Earth, not inconsistent with the 6000 units claimed by Paresce et al., if we include all the uncertainties in both data sets.

5. CONCLUSIONS

We have detected strong line and continuum emission from two targets inside the Eridanus superbubble. From the level of continuum emission we constrain the optical constants of the interstellar dust grains to lie within a fairly narrow range (Fig. 5). These results are inconsistent with those of Murthy et al. (1991). We cannot say whether this is due to uncertainties in the model or due to real differences in the characteristics of the dust.

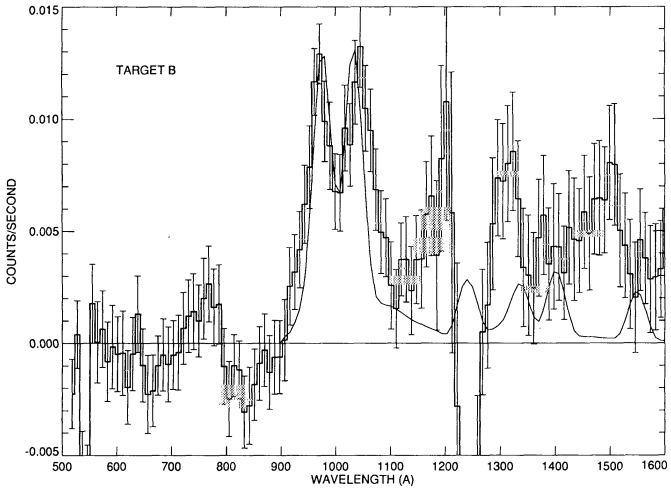

FIG. 7.—The emission expected from a shock with a velocity of 180 km s^{-1}, including two-photon emission, plus the dust scattered continuum of Fig. 7 is superposed on our data from Target B. Although the model does not match the data well above Lyα, the low quality of the data in that spectral region should lead us not to expect much better results. The error bars are $\pm 1\ \sigma$.

We have detected both C III (977 Å) and O VI (1032/1038 Å) emission in Target B, near a peak in the C-band X-ray emission. The line ratios imply a shock velocity on the order of 180 km s^{-1} in this region. Only C III emission is present in Target A with a ratio to Hα consistent with shock velocities of about 100 km s^{-1}. We detect a significant signal above Lyα in Target B which we have identified with a combination of line emission from the shocked gas and a two-photon continuum.

We expect to make several additional observations in Eridanus which will help us to better understand the physical nature of this highly excited region of the ISM. In addition, we are currently in the process of analyzing *Voyager* observations of dust scattering from several regions in the sky, allowing us to further refine our understanding of the optical properties of the dust.

We thank the National Space Science Data Center (NSSDC) for providing the Bright Star Catalog and the H I data on magnetic tape and the IDL Users Astronomy Library at NASA/GSFC for several IDL programs. This research has made use of the SIMBAD database, operated at CDS, Strasbourg, France. We also thank W. P. Blair and O. Vancura for useful discussions. This research has been supported at the Johns Hopkins University by NASA grant NAGW-1890 and at the University of Arizona by NASA grants NAGW-587 and NAGW-2648.

REFERENCES

Blair, W. P., et al. 1991a, ApJ, 379, L33
Blair, W. P., Long, K. S., Vancura, O., & Holberg, J. B. 1991b, ApJ, 374, 202
Bohlin, R. C., Savage, B. D., & Drake, J. F. 1978, ApJ, 224, 132
Burrows, D. N., Singh, K. P., Nousek, J. A., Garmire, G. P., & Good, J. 1993, ApJ, 406, 97
Draine, B. T., & Lee, H. M. 1984, ApJ, 285, 89
Fitzpatrick, E. L., & Massa, D. 1988, ApJ, 328, 734
Gottlieb, D. M. 1978, ApJS, 38, 287
Hartigan, P., Raymond, J., & Hartmann, L. 1987, ApJ, 316, 323
Heiles, C. 1976, ApJ, 208, L137

Holberg, J. B. 1986, ApJ, 311, 969
———. 1990, Proc. IAU 139, The Galactic and Extragalactic Background Radiation, ed. S. Bowyer & Ch. Leinert (Dordrecht: Reidel), 220
———. 1991, Proc. IAU Colloq. 123, Observatories in Earth Orbit and Beyond, ed. Y. Kondo (Dordrecht: Reidel), 49
Holberg, J. B., & Watkins, R. 1992, *Voyager* Ultraviolet Spectrometer Guest Observer and Data Analysis Handbook, Verson 1.1
Murthy, J., Dring, A., Henry, R. C., Kruk, J. W., Blair, W. P., Kimble, R. A., & Durrance, S. T. 1993, ApJ, 408, L97
Murthy, J., Henry, R. C., & Holberg, J. B. 1991, ApJ, 383, 198
Naranan, S., Shulman, S., Friedman, H., & Fritz, G. 1976, ApJ, 208, 718
Paresce, F. 1984, AJ, 89, 1022
Paresce, F., Jakobsen, P., & Bowyer, S. 1983, A&A, 124, 300
Penprase, B. E., Blades, J. C., Danks, A. C., & Crane, P. 1990, ApJ. 365, 241
Reynolds, R. J., & Ogden, P. M. 1979, 229, 942
Reynolds, R. J., Roessler, F. L., & Scherb, F. 1974, ApJ, 192, L53
Sandage, A. 1976, AJ 81, 954
Shemansky, D. E., Sandel, B. R., & Broadfoot, A. L. 1979, ApJ, 231, 35
Shull, J. M., & Van Steenberg, M. E. 1985, ApJ, 294, 599
Sivan, J. P. 1974, A&AS, 16, 163
Snow, T. P., Allen, M. M., & Polidan, R. S. 1990, ApJ, 359, L23
Stark, A. A., Gammie, C. F., Wilson, R. W., Bally, J., Linke, R. A., Heiles, C., & Hurwitz, M. 1992, ApJS, 79, 77
Tucker, W. H., & Koren, M. 1971, ApJ, 168, 283
Williamson, F. O., Sanders, W. T., Kraushaar, W. L., McCammon, D., Borken, R., & Bunner, A. N. 1974, ApJ, 193, L133
Witt, A. N., Petersohn, J. K., Holberg, J. B., Murthy, J., Dring, A., & Henry, R. C. 1993, ApJ, 410, 714